REVISION 1 Word Count: 5886

Paulišite, $Ca_2Zn(CO_3)_3 \cdot 2H_2O$, a new mineral with a novel crystal structure

JIŘÍ SEJKORA[1§], CRISTIAN BIAGIONI[2,3], ZDENĚK DOLNÍČEK[1], RADEK ŠKODA[4] AND JANA EDEROVA[5]

[1]Department of Mineralogy and Petrology, National Museum, Cirkusová 1740, CZ-193 00 Prague 9 - Horní Počernice, Czech Republic

[2]Dipartimento di Scienze della Terra, Università di Pisa, Via Santa Maria, 53, I-56126 Pisa, Italy

[3]Centro per l'Integrazione della Strumentazione Scientifica dell'Università di Pisa, Pisa, Italy

[4]Department of Geological Sciences, Faculty of Science, Masaryk University, Kotlářská 2, CZ-611 37 Brno, Czech Republic

[5]University of Chemistry and Technology Prague, Technická 5, CZ-166 28 Prague 6, Czech Republic

ABSTRACT

Paulišite, $Ca_2Zn(CO_3)_3 \cdot 2H_2O$, is a new mineral species discovered in the underground workings at the abandoned mine adit of the 1st level of the Staročeské Lode, near the historical shaft Šafary, Kaňk near Kutná Hora, central Bohemia, Czech Republic. Paulišite is associated with hydrozincite and aragonite (holotype sample) or with calcite, aragonite, hydrozincite and monohydrocalcite (other samples). The new mineral occurs as crusts, up to 1 cm thick, formed by parallel or radial aggregates of acicular crystals, elongated on [100], up to 5 mm in length.

§ Email:jiri.sejkora@nm.cz

This is the peer-reviewed, final accepted version for American Mineralogist, published by the Mineralogical Society of America.
The published version is subject to change. Cite as Authors (Year) Title. American Mineralogist, in press.
DOI: https://doi.org/10.2138/am-2024-9418. http://www.minsocam.org/

Paulišite is colorless to white, with a white streak. It is transparent and has a vitreous luster. Mohs hardness is *ca*. 4; the calculated density is 2.756 g/cm^3. Paulišite is optically biaxial positive, with α = 1.554(1), β = 1.569(2), and γ = 1.605(1) (589 nm), and $2V_{(meas.)}$ = 68(2)°. The empirical formula, based on electron-microprobe analyses (n = 11), is $Ca_{2.00}(Zn_{0.97}Mg_{0.02}Cu_{0.01}Al_{0.01})_{\Sigma 1.01}(CO_3)_3 \cdot 2H_2O$ on the basis of three cations (excluding C) per formula unit. The ideal formula is $Ca_2Zn(CO_3)_3 \cdot 2H_2O$, which requires (in wt%) CaO 31.02, ZnO 22.50, CO_2 36.51, H_2O 9.97, total 100.00. The strongest reflections of the powder X-ray diffraction pattern [d(Å)/(I_{rel})/hkl] are: 8.226/(100)/011, 6.492/(100)/002, 4.112/(18)/022, 3.246/(35)/004, 3.085/(19)/130, and 2.458/(21)/042. According to single-crystal X-ray diffraction data, paulišite is monoclinic, space group *Ia*, Z = 4 with a = 6.3007(6), b = 10.6236(11), c = 12.9837(12) Å, β = 90.840(5)°, V = 868.99(15) Å^3. The crystal structure was refined to R_1 = 0.0229 for 2330 unique reflections with $F_o > 4\sigma(F_o)$ and 164 refined parameters. It is characterized by Zn(1)-centered tetrahedra, two independent Ca(1)- and Ca(2)-centered polyhedra, and CO_3 groups. Heteropolyhedral Ca-Zn-CO_3 {001} layers occur in paulišite and are connected along **c** through CO_3 groups and Ca(2)-centered polyhedra, as well as H-bonds. Along with minrecordite, skorpionite, and znucalite, paulišite is the fourth mineral containing Ca, Zn, and (CO_3) groups as species-defining elements. Its origin is related to the supergene alteration of ore deposits following the mining activity, probably at low T and basic pH conditions. The mineral and its name, honouring the Czech mineralogist and geologist Petr Pauliš (b. 1956), have been approved by the Commission on New Minerals, Nomenclature and Classification of the International Mineralogical Association (number 2023-031).

Keywords*:* paulišite, new mineral, zinc, carbonate, crystal structure, Kaňk near Kutná Hora,

Czech Republic.

INTRODUCTION

The Kutná Hora Ag-Pb-Zn ore district (central Bohemia, Czech Republic) represents not only an historically significant producer of silver but it is also known for supergene minerals sub-recently formed, during over hundreds of years, especially in strongly weathered medieval mine dumps. The long-known bukovskýite, $Fe^{3+}(AsO_4)(SO_4)(OH)\cdot 9H_2O$ (Bukovský 1915; Novák et al. 1967), was followed by the more recent descriptions of kaňkite, $Fe^{3+}(AsO_4)\cdot 3.5H_2O$ (Čech et al. 1976), zýkaite, $Fe^{3+}{}_4(AsO_4)_3(SO_4)(OH)\cdot 15H_2O$ (Čech et al. 1978), and parascorodite, $Fe^{3+}(AsO_4)\cdot 2H_2O$ (Ondruš et al. 1999).

The investigation of supergene minerals sub-recently formed in mine workings of the Kutná Hora ore district was started much later (Cílek 1990; Pauliš 1993; Malec and Pauliš 1997; Novák 1999). Beside other minerals (glaucocerinite, woodwardite, hydrozincite, monohydrocalcite, etc.), Novák (1999) described an unnamed hydrated Ca-Zn carbonate with apparently wrong, not charge-balanced, chemical formula $Ca_2Zn(CO_3)_2\cdot 2H_2O$. New study on this unnamed phase allowed to determine all necessary data and solve its crystal structure. The new mineral and its name were approved by the Commission on New Minerals, Nomenclature and Classification of the International Mineralogical Association (IMA 2023-031). The name *paulišite* honours the Czech mineralogist and geologist ing. Petr Pauliš (born 29.4.1956, Ústí nad Orlicí) from Kutná Hora, central Bohemia, Czech Republic, for his contribution to mineralogy and economic geology. Ing. Pauliš is the author of numerous published papers (more than 200) and several books; the majority of them are related to the mineralogy of some Czech localities,

68 including the mineralogy of the Kutná Hora ore district (Malec and Pauliš 1997; Pauliš 1993,
69 1998; Pauliš et al. 2015). The mineral symbol of paulišite, in accord with Warr (2021), is Plš.

70 Holotype material (about one cm-sized fragment and a polished section) of paulišite is
71 deposited in the collections of the Department of Mineralogy and Petrology, National Museum in
72 Prague, Cirkusová 1740, 193 00 Praha 9, Czech Republic, under the catalogue number P1P
73 9/2023, and in the collections of the Museo di Storia Naturale of the Università di Pisa, Via
74 Roma 79, Calci (PI), under catalogue number 20064.

75

76 **OCCURRENCE**

77 The samples containing paulišite were discovered by František Novák in 1988
78 underground at the 1st level of the Staročeské Lode in the adit Ch151, *ca*. 20 m north from the
79 historical shaft Šafary (Novák 1999), Kaňk near Kutná Hora, central Bohemia, Czech Republic
80 (GPS coordinates: 49°58'43.23''N 15°16'6.62''E).

81 The Kutná Hora Ag-Pb-Zn ore district represents a hydrothermal vein-type mineralization
82 of Variscan age (Holub et al. 1982). It was one of the main European producers of silver between
83 the 14th and 16th century, with hundreds of mines opened on twelve major lodes. Each lode (also
84 called *pásmo* in Czech or *Zug* in German) represents a hydrothermally altered zone of several
85 hundred meters to about three kilometres in length and dozens of metres in width, with depth
86 ranging between several hundred metres to 1 km, each consisting of several veins (Holub et al.
87 1982). Geologically and mineralogically, two mineral assemblages are present in this ore district.
88 One is "silver-rich" and occurs in the southern part of the ore district, whereas the other, in the
89 northern part, is "pyrite-rich" (Malec and Pauliš 1997). The Staročeské pásmo Lode belongs to
90 the northern pyrite-rich lodes and it is the biggest lode of the Kutná Hora ore district, both in

terms of the amount of extracted ore and the amount of extracted silver (estimated 300 tons of Ag in the period 1480 - 1600). In the sampling site of paulišite, the primary ore mineralization of the Hlavní vein is represented by major pyrite, arsenopyrite, pyrrhotite, sphalerite and minor chalcopyrite and stannite in quartz gangue with minor carbonates (mostly siderite). The full list of minerals (about 250 species) recorded from this area is given on http://www.mindat.org/loc-18419.html.

PHYSICAL AND OPTICAL PROPERTIES

In holotype material, paulišite occurs as crusts, up to 1 cm in thickness (Fig. 1a), formed by parallel- or radial-arranged acicular crystals, elongated on [100], up to 5 mm in length (Fig. 1b), in association with hydrozincite and Zn-bearing aragonite (with 1.2–12.4 wt% ZnO). In other samples with distinct banded texture, paulišite forms several bands composed of crystalline aggregates alternating with thin interlayers of fine-grained Zn-bearing aragonite (Fig. 1c) or elongated crystals, up to 300 μm in length, in association with calcite, aragonite and hydrozincite in monohydrocalcite matrix (Fig. 1d).

Paulišite is colorless to white, sometimes with a bluish tint, with a white streak. It is transparent in transmitted light and it has a vitreous luster. It is not fluorescent under either shortwave or longwave ultraviolet radiation and is brittle with distinct cleavage parallel to the elongation; fracture is conchoidal. The calculated density ($Z = 4$), based on the empirical formula and the unit-cell parameters refined from single-crystal X-ray diffraction data, is 2.756 g/cm^3. Mohs hardness is assumed to be *ca*. 4 on the basis of scratch tests. Paulišite is colorless and non-pleochroic under plane-polarized light. It forms narrow laths to needles with distinct cleavage parallel to elongation and is biaxial positive with $\alpha = 1.554(1)$, $\beta = 1.569(2)$, and $\gamma = 1.605(1)$,

This is the peer-reviewed, final accepted version for American Mineralogist, published by the Mineralogical Society of America.
The published version is subject to change. Cite as Authors (Year) Title. American Mineralogist, in press.
DOI: https://doi.org/10.2138/am-2024-9418. http://www.minsocam.org/

114 measured at 589 nm light. The angle $2V$ determined from extinctions by spindle stage is 68(2)°,
115 which is in good agreement with the value of 67° calculated by the equation of Wright (1951).
116 The optical orientation X^**a** = -3°, Y=**b**, Z^**c** = 5° is based on the morphological assumptions
117 derived from the crystal structure study. Specifically, crystals are alongated along [100], which is
118 the direction of the "columns" composed of edge-shared Ca(1) and Ca(2) polyhedra
119 interconnected by Zn-centered tetrahedra and CO_3^{2-} groups. The prominent cleavage may be
120 along the {011} and {0-11} planes crosscutting the structural channel (see structure description
121 chapter). Birefringence is 0.051 and it has distinct dispersion $r>v$. The Gladstone-Dale
122 compatibility index (Mandarino 1979, 1981) is 0.014 (superior). The mineral is insoluble in water
123 and decomposes in cold dilute HCl with effervescences.
124

125 ## CHEMICAL COMPOSITION

126 Chemical analyses of paulišite were performed using a Cameca SX100 electron
127 microprobe (National Museum, Prague) operating in wavelength-dispersive mode (15 kV, 5 nA
128 and 8 μm wide beam). The following standards and X-ray lines were used to minimize line
129 overlaps: chalcopyrite (Cu$K\alpha$), diopside (Mg$K\alpha$), sanidine (Al$K\alpha$), wollastonite (Ca$K\alpha$) and ZnO
130 (Zn$K\alpha$). Raw intensities were converted to the concentrations of elements using the automatic
131 "PAP" (Pouchou and Pichoir 1985) matrix-correction procedure. Water and CO_2 contents were
132 calculated on the basis of stoichiometry and $2H_2O$ groups, in agreement with the results of the
133 crystal structure analysis. These calculated contents agree well with results of thermogravimetric
134 analysis (see below).

135 Results (average of 11 analyses) are given in Table 1. On the basis of three cations
136 (excluding C) per formula unit, the empirical formula of paulišite is (with rounding errors)

137 $Ca_{2.00}(Zn_{0.97}Mg_{0.02}Cu_{0.01}Al_{0.01})_{\Sigma 1.01}(CO_3)_3 \cdot 2H_2O$. This formula agrees with the ideal one,
138 $Ca_2Zn(CO_3)_3 \cdot 2H_2O$, corresponding to (in wt%) CaO 31.02, ZnO 22.50, CO_2 36.51, H_2O 9.97,
139 total 100.00.
140

141 **THERMOGRAVIMETRIC ANALYSIS**

142 Thermogravimetric data on holotype material were collected at the University of
143 Chemistry and Technology (Prague, Czech Republic) using a Thermobalance SETSYS (Setaram,
144 France) equipped with a mass spectrometer GSD 320 03 OmniStar (Pfeiffer Vacuum, Austria).
145 The sample weighing 10.258 mg was analysed between 30 and 1200 ^{o}C in air with a heating rate
146 10 ^{o}C.min^{-1}. The powdered sample was checked for purity through powder X-ray diffraction
147 (PXRD) and beside dominant paulišite it also contained small admixture (less than 5-10%) of
148 aragonite (see also Fig. 1b). The collected thermogravimetric curve is shown in Figure 2. Three
149 main weight loss steps can be identified: (i) between 30 and 225 °C, (ii) between 225 and 350 °C,
150 and (iii) between 350 and 1200 °C. The first step (2.23 wt. %) corresponds to the loss of *ca*. 0.5
151 H_2O groups. The second weight loss (9.34 wt. %) is connected to dominant dehydration (*ca*. 7.7
152 wt. % ~ 1.5 H_2O groups) and the loss of a small fraction of CO_2 (ca. 1.6 wt. % ~ 0.1 CO_2). The
153 loss of both chemical constituents is documented by mass spectrometry. The reaction product at
154 350 °C is represented by a mixture of carbonate of dolomite-type structure, aragonite and minor
155 calcite. The third step of weight loss (34.09 wt%) corresponds to the full decomposition of
156 carbonates (~ 2.9 CO_2 molecules). The reaction end-product is formed by lime (CaO) and zincite
157 (ZnO). The total observed weight loss, 45.66 wt. % in the range 30 - 1200 °C, is comparable with
158 the ideal H_2O+CO_2 contents in paulišite, i.e., 46.48 wt. %. The small difference between these

159 values is most likely caused by the minor admixture of other mineral phases in measured sample
160 or some analytical uncertainties.
161
162 **RAMAN SPECTROSCOPY**

163 The Raman spectrum of paulišite was collected in the range 4000–30 cm^{-1} using a DXR
164 dispersive Raman Spectrometer (Thermo Scientific) mounted on confocal Olympus microscope
165 (National Museum, Prague). The Raman signal was excited by an unpolarised green diode-
166 pumped solid-state laser (λ = 532 nm) and detected by a CCD detector. The experimental
167 parameters were: 100× objective, 10 s exposure time, 100 exposures, 400 lines/mm grating, 50
168 μm pinhole spectrograph aperture and 8 mW laser power level. The thermal damage of the
169 measured points was excluded by the visual inspection of the excited surface after measurement,
170 by the observation of the possible decay of spectral features in the start of excitation and
171 checking for thermal downshift of Raman lines. The instrument was set up by a software-
172 controlled calibration procedure using multiple neon emission lines (wavelength calibration),
173 multiple polystyrene Raman bands (laser frequency calibration) and standardized white-light
174 sources (intensity calibration). Spectral manipulations were performed using the Omnic 9
175 software (Thermo Scientific). The main observed bands are: 3475, 3420, 3262, 1726, 1708, 1590,
176 1578, 1469, 1379, 1090, 1072, 852, 772, 700, 680, 395, 378, 332, 186, 158, 121, and 77 cm^{-1}.

177 The Raman spectrum of paulišite in the full range is given in Figure 3. Its interpretation is
178 based on the paper by Čejka et al. (2013) and references therein. A broad band with components
179 at 3475, 3420 and 3262 cm^{-1} was assigned to the ν O–H stretching vibrations of the hydrogen-
180 bonded H_2O groups. According to the empirical equation of Libowitzky (1999), O–H···O
181 hydrogen bond lengths were calculated at approximately 2.87, 2.81 and 2.73 Å, which are

This is the peer-reviewed, final accepted version for American Mineralogist, published by the Mineralogical Society of America.
The published version is subject to change. Cite as Authors (Year) Title. American Mineralogist, in press.
DOI: https://doi.org/10.2138/am-2024-9418. http://www.minsocam.org/

comparable with values inferred from crystal structure data. Weak bands at 1726 and 1708 cm^{-1} can be related to combination bands/overtones. Weak bands at 1590, 1578, 1469 and 1379 cm^{-1} are attributed to the doubly degenerate ν_3 CO_3^{2-} antisymmetric stretching vibrations, and a strong band at 1090 with a shoulder at 1072 cm^{-1} to the ν_1 CO_3^{2-} symmetric stretching vibrations. For the bands at 1590 and 1578 cm^{-1}, an overlapping of the ν_3 CO_3^{2-} and the ν_2 (δ) bending vibrations of H_2O is supposed. Very weak band at 852 cm^{-1} is related to the ν_2 (δ) CO_3^{2-} out-of-plane bending vibration. However, some overlap with libration modes of H_2O groups may be expected. Weak bands at 772, 700 and 680 cm^{-1} are attributed to the doubly degenerate ν_4 (δ) CO_3^{2-} in-plane bending vibrations. The bands in the range 400–100 cm^{-1} (395, 378, 332, 186, 158, 121 cm^{-1}) can be related to vibrations of bonds at $M^{2+}(O,H_2O)_n$ polyhedra, whereas the band at 74 cm^{-1} is due to lattice mode.

X-RAY CRYSTALLOGRAPHY AND STRUCTURE DETERMINATION

Single-crystal X-ray diffraction data of paulišite were collected using a Bruker D8 Venture four-circle diffractometer equipped with an air-cooled Photon III detector, and microfocus Mo$K\alpha$ radiation (Centro per l'Integrazione della Strumentazione Scientifica dell'Università di Pisa, Pisa, Italy). The detector-to-crystal distance was set to 38 mm. Data were collected using ω and φ scan modes, in 0.5° slices, with an exposure time of 30 s per frame. A total of 1312 frames were collected and they were integrated with the Bruker SAINT software package using a narrow-frame algorithm. Data were corrected for Lorentz-polarization, absorption, and background. Unit-cell parameters, refined on the basis of the XYZ centroids of 5335 reflections above 20 σI with 4.96° < 2θ < 60.58°, are a = 14.3484(12), b = 10.6236(11), c = 6.3007(6) Å, β = 115.205(4)°, V = 868.98(14) $Å^3$. The statistical tests on the distribution of |E|

This is the peer-reviewed, final accepted version for American Mineralogist, published by the Mineralogical Society of America.
The published version is subject to change. Cite as Authors (Year) Title. American Mineralogist, in press.
DOI: https://doi.org/10.2138/am-2024-9418. http://www.minsocam.org/

values ($|E^2 - 1| = 0.751$) suggest the absence of a center of symmetry. Considering also the systematic absences, the crystal structure of paulišite was solved in the space group *Cc* using ShelxTL and was refined using *Shelxl*-2018 (Sheldrick 2015). This non-standard cell was later transformed into a standard monoclinic cell (e.g., Mighell 2002), with unit-cell parameters a = 6.3007(6), b = 10.6236(11), c = 12.9837(12) Å, β = 90.840(5)°, V = 868.99(15) Å^3, space group *Ia*.

Six cation sites and eleven oxygen positions were located. Cation sites are represented by a Zn-centered tetrahedron, two nine- and ten-fold coordinated Ca-centered polyhedra, and three C sites. Neutral scattering curves for Zn, Ca, C, and O sites were taken from the *International Tables for Crystallography* (Wilson 1992). Racemic twinning was modelled, supporting the absence of a center of symmetry. Difference-Fourier maps allowed the location of some H atoms, In particular, four maxima around O(6) and O(11) atoms were found. Their O–H distances were restrained to be ca. 1.00 Å, whereas displacement parameters were constrained to be 1.5 times those of the bonded O atoms. However, one of the H atoms bonded at O(11) was too close to Ca(2) (i.e., 2.56(6) Å) and the H–O–H angle was too small (i.e., ca. 87°). For this reason, such an H atom was removed from the final structural model. The anisotropic structural model of paulišite converged to R_1 = 0.0229 for 2330 reflections with $F_o > 4\sigma(F_o)$ and 164 refined parameters. Details of data collection and refinement are given in Table 2. Fractional atom coordinates and equivalent isotropic displacement parameters are reported in Table 3. Table 4 reports selected bond distances, whereas bond-valence sums (BVS), calculated according to Brese and O'Keeffe (1991), are shown in Table 5. The details of the data collection, crystallographic parameters and the fit statistics are given within the cif file provided as Supplementary material.

This is the peer-reviewed, final accepted version for American Mineralogist, published by the Mineralogical Society of America.
The published version is subject to change. Cite as Authors (Year) Title. American Mineralogist, in press.
DOI: https://doi.org/10.2138/am-2024-9418. http://www.minsocam.org/

Powder X-ray diffraction data were collected at room temperature using a Bruker D8 Advance diffractometer equipped with a solid-state LynxEye detector and secondary monochromator producing Cu*K*α radiation (Department of Mineralogy and Petrology, National Museum, Prague, Czech Republic). The instrument was operating at 40 kV and 40 mA. In order to minimize the background, the powder samples were placed on the surface of a flat silicon wafer. The powder pattern was collected using a Bragg–Brentano geometry in the range 3–65° 2θ, step 0.01° and counting time of 20 s per step (total duration of experiment was *ca*. 30 hours). The positions and intensities of diffraction effects were found and refined using the Pearson VII profile-shape function of the ZDS program package (Ondruš 1993). Data are given in Table 6. Differences between observed and calculated diffraction intensity are caused by preferred orientation and other textural effects. Unit-cell parameters were refined by the least-squares program of Burnham (1962) in the monoclinic space group *Cc* (#9) as follows: $a = 6.3032(6)$, $b = 10.6258(8)$, $c = 12.9838(9)$ Å, $\beta = 90.747(8)°$, $V = 869.50(9)$ Å^3 and $Z = 4$.

CRYSTAL STRUCTURE DESCRIPTION

The crystal structure of paulišite (Fig. 4) is characterized by Zn(1)-centered tetrahedra, Ca(1)- and Ca(2)-centered polyhedra, and three symmetry-independent CO_3 groups.

General features

The connection between Zn(1)-centered tetrahedra and C(3)O_3 groups forms chains running along **a**. These heteropolyhedral chains are connected, along **b**, through edge-sharing and additional C(1)O_3 groups, with columns of Ca(1)-centered polyhedra connected through face-

250 sharing. In this way, {001} heteropolyhedral Ca-Zn-CO_3 layers can be identified. Along **c**, these
251 layers are connected through $C(2)O_3$ groups and Ca(2)-centered polyhedra.
252
253 **Cation coordination**
254 Zinc is hosted at a tetrahedrally coordinated site, with average <Zn–O> distance of 1.942
255 Å. These values can be compared with those reported for other tetrahedrally coordinated Zn
256 atoms occurring in carbonates, e.g., 1.965 Å in aurichalcite (Giester and Rieck 2014), 1.952 Å in
257 hydrozincite (Ghose 1964), 1.987 and 1.905 Å for two symmetry-independent Zn-centered
258 tetrahedra in loseyite (Hill 1981) and 1.978 and 1.923 Å for the related mineral sclarite (Grice
259 and Dunn 1989). Šlikite displays two tetrahedrally coordinated Zn atoms, with average distances
260 of 1.977 and 1.984 Å (Sejkora et al. 2019). Finally, tetrahedrally coordinated Zn occurs also in
261 the Ca-Zn phosphate-carbonate skorpionite (<Zn–O> = 1.9665 Å – Krause et al. 2008) and in
262 znucalite (<Zn–O> = 1.95 Å – Steciuk et al. 2024). One can see that the average distance
263 observed in paulišite is slightly shorter than those observed in several other carbonates.
264 Moreover, it is also shorter than the value calculated on the basis of the sum of the ionic radii of
265 Shannon (1976) for $^{[IV]}Zn^{2+}$ and O^{2-}, i.e., 1.9625 Å. In agreement with electron microprobe data,
266 the site occupancy at the Zn site was almost pure, with only very minor replacement of Zn by
267 Mg, Cu, and Al. The BVS at this site is 2.11 valence units (v.u.), in accord with the occurrence of
268 Zn^{2+}.
269 Calcium is hosted at two symmetry-independent Ca sites, Ca(1) and Ca(2). The former is
270 ten-fold coordinated, with nine Ca–O bond distances shorter than 2.80 Å (average 2.545 Å) and a
271 longer one at 2.96 Å. Ca(2) is nine-fold coordinated, with average bond distance of 2.524 Å. The
272 BVSs at these Ca sites are 2.05 and 2.10 v.u., respectively, in accord with the presence of Ca^{2+}.

This is the peer-reviewed, final accepted version for American Mineralogist, published by the Mineralogical Society of America.
The published version is subject to change. Cite as Authors (Year) Title. American Mineralogist, in press.
DOI: https://doi.org/10.2138/am-2024-9418. http://www.minsocam.org/

Calcium atoms are coordinated by O^{2-} and H_2O groups, as revealed by BVSs (Table 5), giving rise to $Ca(1)O_9(H_2O)$ and $Ca(2)O_7(H_2O)_2$ polyhedra. In the Ca(1)-centered polyhedron, the longest distance (> 2.80 Å) is formed with the O atom of the H_2O group hosted at O(11), whereas in the Ca(2)-centered polyhedron, the distances with the O atoms at O(6) and O(11), i.e., the O atoms of the H_2O groups, are not the longest ones.

Three independent CO_3 groups occur in the crystal structure of paulišite; their average bond distances range between 1.280 and 1.283 Å; these values agree with the mean value calculated by Zemann (1981) from 34 CO_3 groups in well-refined crystal structure, i.e., 1.284 Å. O–C–O bond angles vary between 116.2(3) and 122.6(3)°. The BVS range between 4.01 and 4.04 v.u., in accord with the occurrence of C^{4+}.

Anion coordination and H-bonds

Eleven anion positions have been identified in the crystal structure of paulišite. On the basis of their BVS (Table 5), they can be distinguished between O atoms (BVS ranging between 1.83 and 2.16 v.u.) and H_2O groups (BVS of 0.19 and 0.37 v.u.). The latter are hosted at the O(6) and O(11) positions. Difference-Fourier maps showed the presence of residual maxima at ca. 0.8-1.0 Å from the two underbonded O atoms, i.e., O(6) and O(11). These maxima probably represent H atoms. However, only three H atoms were confidently located. O(6) is bonded to two H atoms, namely H(61) and H(62), with O(6)–H distances of 0.97(3) and 0.95(3) Å, respectively, and an H(61)–O(6)–H(62) angle of 97(5)°. Such an angle is lower than expected for an H_2O group, that has an average angle of ~ 108° (Ferraris and Franchini-Angela 1972), but it was considered as a possible H_2O group in accord with the large uncertainty. H(61) and H(62) are involved in H-bonds with O(9) and O(10), respectively, i.e., O(6)–H(61)···O(9) 3.025(4) Å and

296 bond angle of 146(6)° and O(6)–H(62)···O(10) 2.813(4) Å, with bond angle of 152(6)°. Two
297 residuals around O(11) were also located. However, one of them is too close to Ca(2) and does
298 not form any reasonable H-bond, and it was not included in the refinement. Moreover, it would
299 also form a very narrow H–O–H angle, i.e., 87(7)°. For this reason, only the H(111) atom was
300 added. This H atom forms a very long (= weak) H-bond with O(6), with a O(11)–H(111)···O(6)
301 distance of 3.211(5) Å, and a bond angle of 145(6)°. Probably, an additional H-bond is formed
302 with another O(6) atom, forming an O···O distance of 2.852(5) Å, with an O(6)···O(11)···O(6)
303 angle of ~ 105.18(16)°.
304
305 **RELATIONSHIP TO KNOWN SPECIES**
306 Paulišite does not correspond to any valid or invalid unnamed mineral (Smith and Nickel
307 2007). It is identical with unnamed hydrated Ca-Zn carbonate from the Staročeské Lode, Kaňk
308 near Kutná Hora (Novák 1999). Paulišite represents a new addition to naturally occurring Zn-
309 bearing carbonates (Table 7). In these compounds, Zn occurs mainly in octahedral or tetrahedral
310 coordination, with some compounds being characterized by different coordination environments
311 for Zn (e.g., aurichalcite – Giester and Rieck 2014). Moreover, paulišite is the fourth natural
312 species having Ca, Zn, and (CO_3) groups as species-defining elements, along with minrecordite,
313 skorpionite, and znucalite. However, the two latter phases are characterized by the occurrence of
314 additional chemical constituents. Skorpionite has a (Ca/Zn) atomic ratio of 1.5 and it is
315 characterized by the occurrence of $(PO_4)^{3-}$ groups, along with $(CO_3)^{2-}$, $(OH)^-$, and H_2O groups
316 (Krause et al. 2008). Znucalite has a very high Zn content with respect to Ca (Zn/Ca = ~ 12) and
317 it has the $(UO_2)^{2+}$ cation (Ondruš et al. 1990; Steciuk et al. 2024). Minrecordite, on the contrary,

318 belongs to the quaternary system CaO–ZnO–CO_2–H_2O, along with paulišite, and it is the Zn-
319 analogue of dolomite (Garavelli et al. 1982).
320
321 **ORIGIN OF PAULIŠITE**
322 Paulišite is a post-mining supergene mineral. It formed at temperatures of 8-10°C, in
323 conditions probably similar to those of the closely associated hydrozincite. This latter mineral is
324 usually formed from aqueous solution with a wide range of P_{CO2}, around equilibrium with
325 atmosphere, in neutral to basic *p*H conditions (e.g., Alwan and Williams 1979; Preis and
326 Gamsjäger 2001; Reichert and Borg 2008). In some samples, paulišite is associated with
327 monohydrocalcite, a phase that is metastable with respect to both calcite and aragonite. Its
328 formation is related to *p*H > 8 and higher Mg/Ca ratio than those occurring during the
329 crystallization of the anhydrous Ca-carbonates (Fukushi et al. 2011; Munemoto and Fukushi
330 2008; Nishiyama et al. 2013).
331 On the basis of the observed mineral association, it is probable that paulišite crystallized
332 in a low *T*, basic environment, but the actual conditions favouring its crystallization instead of a
333 mixture of hydrozincite and aragonite or calcite are not known. To the best of our knowledge,
334 $Ca_2Zn(CO_3)_3 \cdot 2H_2O$ has not been obtained in synthetic runs and it could occur as a metastable
335 compound, like other naturally occurring carbonates (e.g., aragonite – Sun et al. 2015).
336 Unfortunately, the sampling site of paulišite is inaccessible today and it is not possible to obtain
337 enough pure material for thermodynamic measurements.
338
339 **IMPLICATIONS**

Considering its concentration in the continental crust, zinc is the 22nd element in order of abundance (65 μg/g – Wedepohl 1995) and it usually occurs in sphalerite. Upon weathering of sulfide ores, several supergene phases (mainly represented by carbonates and silicates) rapidly form. Paulišite is a new addition to the systematics of supegene Zn minerals. Its crystallization in supergene environments rules the fate and dispersion of Zn, and represents a new kind of geological CO_2-sequestration in the critical zone, where ore deposits are affected by the interaction with atmosphere, hydrosphere, and biosphere.

From a crystal structure perspective, paulišite is a new carbonate mineral showing a novel atomic arrangement. Its findings stress the role of the study of natural mineral associations in discovering chemical compounds not yet synthesized in the laboratory experiments. This agrees with previous observations by other authors about the predictive power of synthetic compounds. Indeed, the latter is less than one might expect. For instance, Grew et al. (2017) noted that more than half of new B-bearing minerals have never been synthesized or had not been known as synthetic compounds at the time of discovery.

Paulišite has not previously synthesized nor theorized on the basis of thermodynamic data. Its finding is a further proof that "theory will take you only so far" and that crystal chemical investigations of natural samples is still a fertile field of research, allowing a better understanding of the way our planet works.

ACKNOWLEDGEMENTS

We thank Petr Pauliš for providing samples from findings of František Novák († 2009) for this research and express our gratitude to Ian Grey, Anatoly Kasatkin, and an anonymous reviewer as well as to the Associate Editor Fabrizio Nestola for their constructive comments,

which improved the manuscript. The Centro per l'Integrazione della Strumentazione Scientifica dell'Università di Pisa is acknowledged for the access to the X-ray laboratory.

FUNDING

This research was financially supported by the Ministry of Culture of the Czech Republic (long-term project DKRVO 2024-2028/1.II.a; National Museum, 00023272).

REFERENCES CITED

Alwan, A.K., and Williams, P.A. (1979) Mineral formation from aqueous solution. Part I. The deposition of hydrozincite, $Zn_5(OH)_6(CO_3)_2$, from natural waters. Transition Metal Chemistry, 4, 128-132.

Brese, N.E., and O'Keeffe, M. (1991) Bond-valence parameters for solids. Acta Crystallographica, B47, 192-197.

Bukovský, A. (1915) The Poisonous Earth from Kutná Hora. Dvanáctá výroční zpráva c. k. státní reálky v Nymburce za školní rok 1914-15, 3-4. Nymburk. (in Czech)

Burnham, C.W. (1962) Lattice constant refinement. Carnegie Institute Washington Yearbook, 61, 132–135.

Čech, F., Jansa, J., and Novák, F. (1976) Kaňkite, $FeAsO_4 \cdot 3½H_2O$, a new mineral. Neues Jahrbuch für Mineralogie, Monatshefte, 1976, 426-436.

Čech, F., Jansa, J., and Novák, F. (1978) Zýkaite, $Fe^{3+}{}_4(AsO_4)_3(SO_4)(OH) \cdot 15H_2O$, a new mineral. Neues Jahrbuch für Mineralogie - Monatshefte, 1978, 134-144.

Čejka, J., Sejkora, J., Jebavá, I., Xi Y. Couperthwaite, S., and Frost, R.L. (2013) A Raman spectroscopic study of the basic carbonate mineral callaghanite $Cu_2Mg_2(CO_3)(OH)_6.2H_2O$. Spectrochimica Acta A108, 171-176.

Cílek, V. (1990) Kutná Hora - karst and historical underground. Speleofórum, 1990, 8-10. (in Czech)

Dunn, J., Peacor, R., and Sturman, B. D. (1980) Hauckite, $Fe^{3+}_3(Mg,Mn)_{24}Zn_{18}(SO_4)_4(CO_3)_2(OH)_{81}$ a new mineral from Sterling Hill, New Jersey. American Mineralogist, 65, 192-195.

Effenberger, H., Mereiter, K., and Zemann, J. (1981) Crystal structure refinements of magnesite, calcite, rhodochrosite, siderite, smithsonite, and dolomite, with discussion of some aspects of the stereochemistry of calcite type carbonates. Zeitschrift fur Kristallographie, 156, 233-243.

Ferraris, G., and Franchini-Angela, M. (1972) Survey of the geometry and environment of water molecules in crystalline hydrates studied by neutron diffraction. Acta Crystallographica B28, 3572–3583.

Ferraris, G., and Ivaldi, G. (1988) Bond valence vs bond length in O···O hydrogen bonds. Acta Crystallographica, B44, 341-344.

Flack, H.D. (1983) On enantiomorph-polarity estimation. Acta Crystallographica, A39, 876-881.

Fukushi, K., Munemoto, T., Sakai, M., and Yagi, S. (2011) Monohydrocalcite: a promising remediation material for hazardous anions. Science and Technology of Advanced Materials, 12, 064702.

Garavelli, C.G., Vurro, F., and Fioravanti, G.C. (1982) Minrecordite: a New Mineral from Tsumeb [Namibia]. The Mineralogical Record, 13, 131-136.

Giester, G., and Rieck, B. (2014) Crystal structure refinement of aurichalcite, $(Cu,Zn)_5(CO_3)_2(OH)_6$, from the Lavrion Mining District, Greece. Neues Jahrbuch für Mineralogie, Abhandlungen, 191, 225-232.

Ghose, S. (1964) The crystal structure of hydrozincite, $Zn_5(OH)_6(CO_3)_2$. Acta Crystallographica, 17, 1051-1057.

Grew, E.S., Hystad, G., Hazen, R.M., Krivovichev, S.V., and Gorelova, L.A. (2017) How many boron minerals occur in Earth's upper crust? American Mineralogist 102, 1573-1587.

Grice, J.D., and Dunn, P.J. (1989) Sclarite, a new mineral from Franklin, New Jersey, with essential octahedrally and tetrahedrally coordinated zinc: Description and structure refinement. American Mineralogist, 74, 1355-1359.

Hill, R.J. (1981) The structure of loseyite. Acta Crystallographica, B37, 1323-1328.

Holub, M., Hoffman, V., Mikuš, V., and Trdlička, Z. (1982) Polymetallic mineralization of the Kutná Hora ore district. Sborník geologických věd, ložisková geologie, mineralogie, 23, 69-123. (in Czech)

Kraus, W., and Nolze, G. (1996) POWDER CELL – a program for the representation and manipulation of crystal structures and calculation of the resulting X-ray powder patterns. Journal of Applied Crystallography, 29, 301-303.

Krause, W., Effenberger, H., Bernhardt, H.J., and Medenbach, O. (2008) Skorpionite, $Ca_3Zn_2(PO_4)_2CO_3(OH)_2 \cdot H_2O$, a new mineral from Namibia: description and crystal structure. European Journal of Mineralogy 20, 271-280.

Libowitzky, E. (1999) Correlation of O-H stretching frequencies and O-H···O hydrogen bond lengths ln Minerals. Monatshefte für Chemie 130, 1047-1059.

Livingstone, A., and Champness, P.E. (1993) Brianyoungite, a new mineral related to hydrozincite, from the north of England ore field. Mineralogical Magazine, 57, 665-670.

Lozano, R.P., Rossi, C., La Iglesia, Á., and Matesanz, E. (2012) Zaccagnaite-3R, a new Zn-Al hydrotalcite polytype from El Soplao cave (Cantabria, Spain). American Mineralogist, 97, 513-523.

Malec, J., and Pauliš, P. (1997) The Kutná Hora ore district and manifestations of defunct mining and metallurgical activities on its territory. Bulletin mineralogicko-petrologického oddělení Národního muzea v Praze, 4-5, 84-105. (in Czech)

Mandarino, J.A. (1979) The Gladstone-Dale relationship. Part III. Some general applications. The Canadian Mineralogist, 17, 71-76.

Mandarino, J.A. (1981) The Gladstone-Dale relationship. Part IV. The compatibility concept and its application. The Canadian Mineralogist, 19, 441-450.

Merlino, S., and Orlandi, P. (2001) Carraraite and zaccagnaite, two new minerals from the Carrara marble quarries: their chemical compositions, physical properties, and structural features. American Mineralogist, 86, 1293-1301.

Mighell, A.D. (2002) Conventional Cells – The last step toward general acceptance of standard conventional cells for the reporting of crystallographic data. Journal of Research of the National Institute of Standards and Technology 107, 373-377.

Munemoto, T., and Fukushi, K. (2008) Transformation kinetics of monohydrocalcite to aragonite in aqueous solutions. Journal of Mineralogical and Petrological Sciences, 103, 345-349.

Nishiyama, R., Munemoto, T., and Fukushi, K. (2013) Formation condition of monohydrocalcite from $CaCl_2$–$MgCl_2$–Na_2CO_3 solutions. Geochimica et Cosmochimica Acta, 100, 217-231.

Novák, F. (1999) Recent secondary mineral of Staročeské pásmo vein system in the Kutná Hora ore district (central Bohemia). Bulletin mineralogicko-petrologického oddělení Národního Muzea v Praze, 7, 109-117. (in Czech).

Novák, F., Povondra, P., and Vtělenský, J. (1967) Bukovskýit, $Fe^{3+}_2(AsO_4)(SO_4)(OH)\cdot 7H_2O$, from Kaňk, near Kutná Hora, a new mineral. Acta Universitatis Carolinae, Geologica, 4, 297- 325.

Ondruš, P. (1993) A computer program for analysis of X-ray powder diffraction patterns. Materials Science Forum, EPDIC-2, Enchede, 133-136, 297-300.

Ondruš, P., Veselovský, F., and Rybka, R. (1990) Znucalite, $Zn_{12}(UO_2)Ca(CO_3)_3(OH)_{22}\cdot 4H_2O$, a new mineral from Príbram, Czechoslovakia. Neues Jahrbuch für Mineralogie, Monatshefte 1990, 393-400.

Ondruš, P., Skála, R., Viti, C., Veselovský, F., Novák, F., and Jansa, J. (1999) Parascorodite, $FeAsO_4\cdot 2H_2O$ - a new mineral from Kaňk near Kutná Hora, Czech Republic. American Mineralogist, 84(9), 1439-1444.

Pauliš, P. (1993) Secondary sulfates from Kaňk near Kutná Hora. Věstník Českého geologického ústavu, 68(3), 47-48. (in Czech)

Pauliš, P. (1998) Minerals of the Kutná Hora ore district. 50 pp. Kuttna, Kutná Hora.

Pauliš, P., Malíková, R., and Pour, O. (2015) Boyleite from medieval dumps of the Staročeské lode at Kaňk near Kutná Hora (Czech Republic). Bulletin mineralogicko-petrologického oddělení Národního muzea v Praze, 23, 43-45. (in Czech)

Perchiazzi, N., Demitri, N., Fehér, B., and Vignola, P. (2017) On the crystal-chemistry of rosasite and parádsasvárite. The Canadian Mineralogist, 55, 1027-1040.

Pouchou, J.L., and Pichoir, F. (1985) "PAP" (φρZ) procedure for improved quantitative microanalysis. Pp. 104-106 in: Microbeam Analysis (J.T. Armstrong, editor). San Francisco Press, San Francisco.

Preis, W., and Gamsjäger, H. (2001) (Solid + solute) phase equilibria in aqueous solution. XIII. Thermodynamic properties of hydrozincite and predominance diagrams for (Zn^{2+}+ H_2O+ CO_2). The Journal of Chemical Thermodynamics, 33, 803-819.

Reichert, J., and Borg, G. (2008) Numerical simulation and a geochemical model of supergene carbonate-hosted non-sulphide zinc deposits. Ore Geology Reviews, 33, 134-151.

Sejkora, J., Grey, I.E., Kampf, A.R., Mumme, W.G., Bureš, B., and Čejka, J. (2019) Šlikite, $Zn_2Mg(CO_3)_2(OH)_2{\cdot}4H_2O$, a new Zn – Mg carbonate from Plavno, Jáchymov ore district, Czech Republic. European Journal of Mineralogy, 31, 1047-1054.

Shannon, R.D. (1976) Revised effective ionic radii and systematic studies of interatomic distances in halides and chalcogenides. Acta Crystallographica A32, 751-767.

Sheldrick, G.M. (2015) Crystal structure refinement with SHELXL. Acta Crystallographica, C71, 3-8.

Smith, D.G.W., and Nickel, E.H. (2007) A system for codification for unnamed minerals: report of the Subcommittee for Unnamed Minerals of the IMA Commission on New Minerals, Nomenclature and Classification. The Canadian Mineralogist, 45, 983-1055.

Steciuk, G., Majzlan, J., Rohlíček, J., Škoda, R., Sejkora, J., and Plášil, J. (2024) Znucalite, the only known zinc uranyl carbonate: Its crystal structure and environmental implications. American Mineralogist 109, doi:10.2138/am-2023-8956.

Strunz, H. (1959) Tsumeb, seien Erze und Sekundärmineralien, insbesondere der neu aufgeschlossenen zweiten Oxydationszone. Fortschritte der Mineralogie, 37, 87-90.

Sun, W., Jayaraman, S., Chen, W., Persson, K.A., and Ceder, G. (2015) Nucleation of metastable aragonite $CaCO_3$ in seawater. Proceedings of the National Academy of Sciences, 112, 3199-3204.

Warr, L.N. (2021) IMA-CNMNC approved mineral symbols. Mineralogical Magazine 85, 291-320.

Wedepohl, K.H. (1995) The composition of the continental crust. Geochimica et Cosmochimica Acta 59, 1217-1232.

Wilson, A.J.C. (editor) (1992) International Tables for Crystallography Volume C: Mathematical, Physical and Chemical Tables. Kluwer Academic Publishers, Dordrecht, The Netherlands.

Wright, F. E. (1951). Computation of the optic axial angle from the three principal refractive indices. American Mineralogist, 36(7-8), 543-556.

Yang, H., Gibbs, R.B., Schwenk, C., Xie, X., Gu, X., Downs, R.T., and Evans, S.H. (2021) Liudongshengite, $Zn_4Cr_2(OH)_{12}(CO_3)\cdot 3H_2O$, a new mineral of the hydrotalcite supergroup, from the 79 mine, Gila County, Arizona, USA. The Canadian Mineralogist, 59, 763-769.

Zemann, J. (1981) Zur Stereochemie der Karbonate. Fortschritte Mineralogie 59, 95-116.

FIGURE CAPTIONS

Figure 1. a) Crust formed by acicular paulišite crystals (Plš) with a thin hydrozincite (Hznc) layer and light blue hydrozincite at the contact with rock (holotype sample); **b)** acicular crystals of paulišite with Zn-containing aragonite (Arg) aggregates and hemispherical aggregates of hydrozincite, BSE photo (holotype sample); **c)** paulišite crust with thin layers of fine-grained Zn-bearing aragonite and intergrowths of hydrozincite and aragonite at the contact with rock; **d)**

519 elongated crystals of paulišite in association with calcite (Cal), aragonite and hydrozincite in
520 monohydrocalcite (Mhcal) matrix, BSE photo.

521 **Figure 2.** Thermogravimetric curve for paulišite.

522 **Figure 3.** Raman spectrum of paulišite in the full range (4000–30 cm^{-1}, split at 2000 cm^{-1}).

523 **Figure 4.** Crystal structure of paulišite. (a) The {001} heteropolyhedral layer as seen down **c**. (b)
524 Structure as seen down **a**, with {001} layers connected through Ca(2) polyhedra, CO_3 groups,
525 and H-bonds (not shown). Zn- and Ca(1)-centered polyhedra are shown in light grey and cyan,
526 respectively, whereas CO_3 groups are shown as black polyhedra. Ca(2) is shown as blue ball-and-
527 sticks. O sites hosting O^{2-} atoms are red circles, whereas sites hosting O atoms belonging to H_2O
528 groups are shown as cyan circles. H atoms are not shown.

529

530 TITLES TO TABLES

531

532 **Table 1.** Chemical composition of paulišite (in wt.%).

533 **Table 2.** Crystal and experimental data for paulišite.

534 **Table 3.** Atoms, fractional atom coordinates, equivalent isotropic or isotropic (*) displacement
535 parameters ($Å^2$) for paulišite.

536 **Table 4.** Selected bond distances (in Å) for paulišite.

537 **Table 5.** Bond-valence sums (in valence unit) in paulišite.

538 **Table 6.** X-ray powder diffraction data (*d* in Å) for paulišite; the six strongest observed
539 reflections are shown in bold.

540 **Table 7.** Comparison between paulišite and currently valid Zn-bearing carbonates.

541

542

543 **Table 1.** Chemical composition of paulišite (in wt.%).

544

Constituent	Mean	Range (n = 11)	St.dev.
CaO	30.84	30.37-31.89	0.49
MgO	0.17	0-0.53	0.19
ZnO	21.70	21.36-22.09	0.23
CuO	0.12	0-0.26	0.12
Al_2O_3	0.10	0-0.20	0.07
CO_2*	36.28	35.90-36.96	0.30
H_2O*	9.90	9.79-10.09	0.08
Total	99.11		

545

546 *Notes:* contents of H_2O* and CO_2* were calculated on the basis of the ideal composition (H = 4
547 apfu and C = 3 apfu) derived from the results of the crystal structure study (see below). n =
548 number of spot analyses.

549

Table 2. Crystal and experimental data for paulišite.

Crystal data	
Crystal size (mm)	0.115 × 0.010 × 0.010
Cell setting, space group	Monoclinic, *Ia*
a (Å)	6.3007(6)
b (Å)	10.6236(11)
c (Å)	12.9837(12)
β (°)	90.840(5)
V (Å^3)	868.99(15)
Z	4
Data collection and refinement	
Radiation, wavelength (Å)	Mo*K*α, λ = 0.71073
Temperature (K)	293(2)
$2\theta_{max}$ (°)	60.99
Measured reflections	13430
Unique reflections	2501
Reflections with $F_o > 4\sigma(F_o)$	2330
R_{int}	0.0415
$R\sigma$	0.0356
Range of *h*, *k*, *l*	$-8 \le h \le 8$, $-14 \le k \le 15$, $-18 \le l \le 18$
R [$F_o > 4\sigma(F_o)$]	0.0229
R (all data)	0.0260
wR (on F_o^2)*	0.0500
Goof	0.997
Absolute structure**	0.033(13)
Number of least-squares parameters	164
Maximum and minimum residual peak (*e* Å^{-3})	0.40 [at 0.74 Å from H(111)] -0.36 [at 0.31 Å from H(62)]

*$w = 1/[\sigma^2(F_o^2)+(0.0248P)^2]$.

**Flack (1983).

This is the peer-reviewed, final accepted version for American Mineralogist, published by the Mineralogical Society of America.
The published version is subject to change. Cite as Authors (Year) Title. American Mineralogist, in press.
DOI: https://doi.org/10.2138/am-2024-9418. http://www.minsocam.org/

586 **Table 3.** Atoms, fractional atom coordinates, equivalent isotropic or isotropic (*) displacement
587 parameters ($Å^2$) for paulišite.

588

Site	*x*/*a*	*y*/*b*	*z*/*c*	$U_{eq/iso}$
Zn(1)	0.09652(4)	0.40494(4)	-0.54691(3)	0.01266(10)
Ca(1)	0.38152(10)	0.09344(7)	-0.44649(6)	0.01411(15)
Ca(2)	0.07215(11)	0.76665(7)	-0.19517(6)	0.01366(14)
C(1)	-0.1359(6)	0.1747(3)	-0.5306(3)	0.0130(7)
C(2)	0.1789(5)	0.4697(3)	-0.7528(3)	0.0117(7)
C(3)	-0.0178(6)	0.6304(3)	-0.4401(3)	0.0135(7)
O(1)	0.3769(4)	0.3282(3)	-0.5224(2)	0.0167(6)
O(2)	0.1873(4)	0.5481(3)	-0.8279(2)	0.0151(5)
O(3)	-0.2999(4)	0.1072(3)	-0.5536(2)	0.0194(6)
O(4)	-0.1358(4)	0.2890(2)	-0.5659(2)	0.0174(5)
O(5)	0.0161(4)	0.1301(3)	-0.4790(2)	0.0218(6)
O(6)	0.4196(5)	0.6718(3)	-0.2660(3)	0.0307(7)
H(61)	0.402(11)	0.627(5)	-0.330(3)	0.046*
H(62)	0.535(8)	0.723(5)	-0.287(5)	0.046*
O(7)	0.0248(5)	0.7105(3)	-0.3719(2)	0.0227(6)
O(8)	0.1059(4)	0.5113(2)	-0.6668(2)	0.0156(5)
O(9)	0.0356(5)	0.5156(3)	-0.4313(2)	0.0211(6)
O(10)	0.2399(5)	0.3563(2)	-0.7632(2)	0.0156(5)
O(11)	-0.1857(6)	0.6007(3)	-0.1726(3)	0.0374(9)
H(111)	-0.218(12)	0.515(3)	-0.193(5)	0.056*

589
590

591

This is the peer-reviewed, final accepted version for American Mineralogist, published by the Mineralogical Society of America.
The published version is subject to change. Cite as Authors (Year) Title. American Mineralogist, in press.
DOI: https://doi.org/10.2138/am-2024-9418. http://www.minsocam.org/

592 **Table 4.** Selected bond distances (in Å) for paulišite.

593

Zn(1)	–O(8)	1.925(3)	Ca(1)	–O(5)	2.367(3)
	–O(4)	1.926(3)		–O(7)	2.463(3)
	–O(9)	1.949(3)		–O(3)	2.463(3)
	–O(1)	1.968(3)		–O(2)	2.487(3)
	average	1.942		–O(2)	2.495(3)
				–O(5)	2.559(3)
C(1)	–O(5)	1.254(5)		–O(10)	2.610(3)
	–O(3)	1.289(4)		–O(1)	2.682(3)
	–O(4)	1.297(4)		–O(3)	2.782(3)
	average	1.280		average	2.545
				–O(11)	2.961(4)
C(2)	–O(10)	1.272(5)	Ca(2)	–O(7)	2.385(3)
	–O(2)	1.284(4)		–O(8)	2.396(3)
	–O(8)	1.292(5)		–O(11)	2.418(3)
	average	1.283		–O(10)	2.452(3)
				–O(4)	2.483(3)
C(3)	–O(7)	1.254(5)		–O(6)	2.591(4)
	–O(9)	1.270(5)		–O(3)	2.618(3)
	–O(1)	1.325(4)		–O(1)	2.655(3)
	average	1.283		–O(2)	2.722(3)
				average	2.524

594

595

596 **Table 5.** Bond-valence sums (in valence unit) in paulišite.

597

Site	Zn(1)	Ca(1)	Ca(2)	C(1)	C(2)	C(3)	Σ_{anions}	H-bond	Σ_{anions}*	Theor.
O(1)	0.49	0.14	0.16			1.19	1.98	-	1.98	2.00
O(2)		0.25	0.13		1.33		1.95	-	1.95	2.00
		0.24								
O(3)		0.26	0.17	1.31			1.85	-	1.85	2.00
		0.11								
O(4)	0.55		0.25	1.29			2.09	-	2.09	2.00
O(5)		0.34		1.44			1.98	-	1.98	2.00
		0.20								
O(6)			0.19				0.19	-0.13, -0.18	0.15*	0.00
								+0.10 +0.17		
O(7)		0.26	0.32			1.44	2.02	-	2.02	2.00
O(8)	0.55		0.31		1.30		2.16	-	2.16	2.00
O(9)	0.52					1.38	1.90	+0.13	2.03*	2.00
O(10)		0.18	0.27		1.38		1.83	+0.18	2.01*	2.00
O(11)		0.07	0.30				0.37	-0.10, -0.17	0.10*	0.00
Σcations	2.11	2.05	2.10	4.04	4.01	4.01				
Theor.	2.00	2.00	2.00	4.00	4.00	4.00				

598 *corrected for H-bonds according to Ferraris and Ivaldi (1988).

599

This is the peer-reviewed, final accepted version for American Mineralogist, published by the Mineralogical Society of America.
The published version is subject to change. Cite as Authors (Year) Title. American Mineralogist, in press.
DOI: https://doi.org/10.2138/am-2024-9418. http://www.minsocam.org/

Table 6. X-ray powder diffraction data (d in Å) for paulišite; the six strongest observed reflections are shown in bold.

I_{obs}	d_{obs}	d_{calc}	I_{calc}*	h	k	l	I_{obs}	d_{obs}	d_{calc}	I_{calc}*	h	k	l
100.0	**8.226**	8.2226	100.0	0	1	1	7.7	2.1640	2.1638	4.4	0	0	6
99.5	**6.492**	6.4914	62.9	0	0	2	5.4	2.1253	2.1260	6.9	1	4	3
3.1	5.421	5.4208	9.1	1	1	0	10.4	2.0943	2.0941	4.3	0	3	5
6.1	4.184	4.1839	33.2	-1	1	2	6.7	2.0925	2.0920	8.4	-2	2	4
1.5	4.138	4.1380	3.8	1	1	2	4.6	2.0688	2.0690	9.0	2	2	4
18.4	**4.112**	4.1113	12.5	0	2	2	11.1	2.0555	2.0556	9.7	0	4	4
11.7	4.009	4.0079	8.0	0	1	3	0.8	2.0311	2.0310	2.7	2	4	0
1.5	3.888	3.8861	6.4	-1	2	1	1.9	2.0136	2.0137	3.9	1	5	0
10.4	3.867	3.8675	30.1	1	2	1	3.3	2.0043	2.0040	2.9	0	2	6
3.3	3.416	3.4169	2.3	0	3	1	1.7	2.0016	2.0019	3.0	1	1	6
35.1	**3.246**	3.2457	15.1	0	0	4	9.4	1.9724	1.9717	10.9	-3	1	2
2.1	3.153	3.1514	10.8	2	0	0	3.8	1.9575	1.9572	11.9	3	1	2
18.8	**3.085**	3.0876	38.5	1	3	0	4.2	1.9336	1.9354	9.5	-3	2	1
12.7	2.973	2.9742	37.2	-1	2	3			1.9338	10.6	2	4	2
8.4	2.950	2.9508	12.9	-2	1	1	11.9	1.9074	1.9075	8.8	0	5	3
		2.9494	12.5	1	2	3	4.6	1.8273	1.8271	4.9	0	1	7
14.8	2.936	2.9346	61.7	2	1	1	3.5	1.8073	1.8069	17.3	3	3	0
5.6	2.821	2.8205	14.5	2	0	0	1.3	1.7947	1.7947	4.7	-2	0	6
14.0	2.797	2.7985	46.0	-1	1	4	1.0	1.7893	1.7888	7.8	-3	2	3
		2.7952	19.0	-1	3	2	1.5	1.7857	1.7856	2.8	-1	4	5
2.5	2.781	2.7814	4.2	1	3	2	4.2	1.7769	1.7773	5.7	-1	3	6
8.8	2.771	2.7710	18.2	1	1	4			1.7766	6.3	1	4	5
4.2	2.741	2.7409	3.4	0	3	3	2.9	1.7717	1.7709	2.1	0	6	0
1.9	2.711	2.7104	8.2	2	2	0	7.7	1.7664	1.7667	13.7	1	3	6
6.1	2.656	2.6563	4.7	0	4	0	2.3	1.7475	1.7476	8.5	-2	5	1
11.5	2.523	2.5223	10.4	0	1	5	4.6	1.7435	1.7442	2.6	2	5	1
4.6	2.4915	2.4919	5.7	-2	1	3	1.7	1.7356	1.7357	5.0	3	3	2
		2.4912	11.7	2	2	2	4.0	1.7287	1.7283	8.3	-2	4	4
20.5	**2.4584**	2.4585	23.6	0	4	2	4.8	1.7151	1.7153	13.1	2	4	4
4.8	2.4083	2.4076	15.2	-1	4	1	3.1	1.7084	1.7085	2.8	0	6	2
4.4	2.4028	2.4032	9.9	1	4	1	3.5	1.6927	1.6925	5.6	-1	2	7
1.3	2.2752	2.2758	4.1	-2	0	4	5.2	1.6446	1.6445	6.7	0	5	5
4.8	2.2443	2.2443	12.3	-1	3	4	1.7	1.6361	1.6360	8.4	-2	5	3
12.3	2.1956	2.1962	24.4	-1	2	5	7.3	1.6231	1.6228	5.8	0	0	8
8.6	2.1791	2.1795	17.5	1	2	5	1.0	1.5892	1.5895	2.6	-2	1	7

This is the peer-reviewed, final accepted version for American Mineralogist, published by the Mineralogical Society of America.
The published version is subject to change. Cite as Authors (Year) Title. American Mineralogist, in press.
DOI: https://doi.org/10.2138/am-2024-9418. http://www.minsocam.org/

602 *I_{calc} - calculated using the software *PowderCell*2.3 (Kraus and Nolze, 1996) on the basis of the

603 structural model given in Tables 3 and 4.

604

605 **Table 7.** Comparison between paulišite and currently valid Zn-bearing carbonates.

606

Mineral	Chemical formula	*a* (Å)	*b* (Å)	*c* (Å)	α (°)	β (°)	γ (°)	s.g.
aurichalcite[1]	$(Zn,Cu)_5(CO_3)_2(OH)_6$	13.79	6.41	5.27	90	101.0	90	$P2_1/m$
brianyoungite[2]	$Zn_3(CO_3,SO_4)(OH)_4$	15.72	6.26	5.43	90	~90	90	unknown
hauckite[3]	$Fe^{3+}{}_3(Mg,Mn^{2+})_{24}Zn_{18}(SO_4)_4(CO_3)_2(OH)_{81}$	9.17	9.17	30.21	90	90	120	$P6/mmm$
hydrozincite[4]	$Zn_5(CO_3)_2(OH)_6$	13.62	6.30	5.42	90	90.8	90	$C2/m$
liudongshengite[5]	$Zn_4Cr_2(OH)_{12}(CO_3)\cdot 3H_2O$	3.11	3.11	22.68	90	90	120	$R\text{-}3m$
loseyite[6]	$(Mn^{2+},Zn,Mg)_4Zn_3(CO_3)_2(OH)_{10}$	16.41	5.54	15.15	90	95.5	90	$A2/a$
minrecordite[7]	$CaZn(CO_3)_2$	4.82	4.82	16.03	90	90	120	$R\text{-}3$
parádsasvárite[8]	$Zn_2(CO_3)(OH)_2$	12.25	9.35	3.17	90	97.7	90	$P2_1/a$
paulišite[9]	$Ca_2Zn(CO_3)_3(H_2O)_2$	6.30	10.62	12.98	90	90.8	90	Ia
sclarite[10]	$Zn_7(CO_3)_2(OH)_{10}$	16.11	5.43	15.04	90	95.5	90	$A2/a$
skorpionite[11]	$Ca_3Zn_2(PO_4)_2(CO_3)(OH)_2\cdot H_2O$	19.05	9.32	6.53	90	92.7	90	$C2/c$
šlikite[12]	$Zn_2Mg(CO_3)_2(OH)_2\cdot 4H_2O$	6.34	6.34	13.92	100.0	92.7	114.9	$P\text{-}1$
smithsonite[13]	$ZnCO_3$	4.65	4.65	15.03	90	90	120	$R\text{-}3c$
zaccagnaite[14, 15]	$Zn_4Al_2(OH)_{12}(CO_3)\ 3H_2O$	3.07	3.07	15.11	90	90	120	$P6_3/mmc$
		3.07	3.07	22.62	90	90	120	$R\text{-}3m$
zincrosasite[16]	$(Zn,Cu)_2(CO_3)(OH)_2$	no data available						
znucalite[17]	$Zn_{12}Ca(UO_2)(CO_3)_3(OH)_{22}\cdot 4H_2O$	10.72	6.26	25.36	90	101.1	90	$P2_1/m$

607

608 s.g. - space group; [1] Giester and Rieck (2014); [2] Livingstone and Champness (1993); [3]

609 Dunn et al. (1980); [4] Ghose (1964); [5] Yang et al. (2021); [6] Hill (1981); [7] Garavelli et al.

610 (1982); [8] Perchiazzi et al. (2017); [9] this paper; [10] Grice and Dunn (1989); [11] Krause et al.

611 (2008); [12] Sejkora et al. (2019); [13] Effenberger et al. (1981); [14] Merlino and Orlandi

612 (2001); [15] Lozano et al. (2012); [16] Strunz (1959); [17] Steciuk et al. (2024).

613

This is the peer-reviewed, final accepted version for American Mineralogist, published by the Mineralogical Society of America.
The published version is subject to change. Cite as Authors (Year) Title. American Mineralogist, in press.
DOI: https://doi.org/10.2138/am-2024-9418. http://www.minsocam.org/

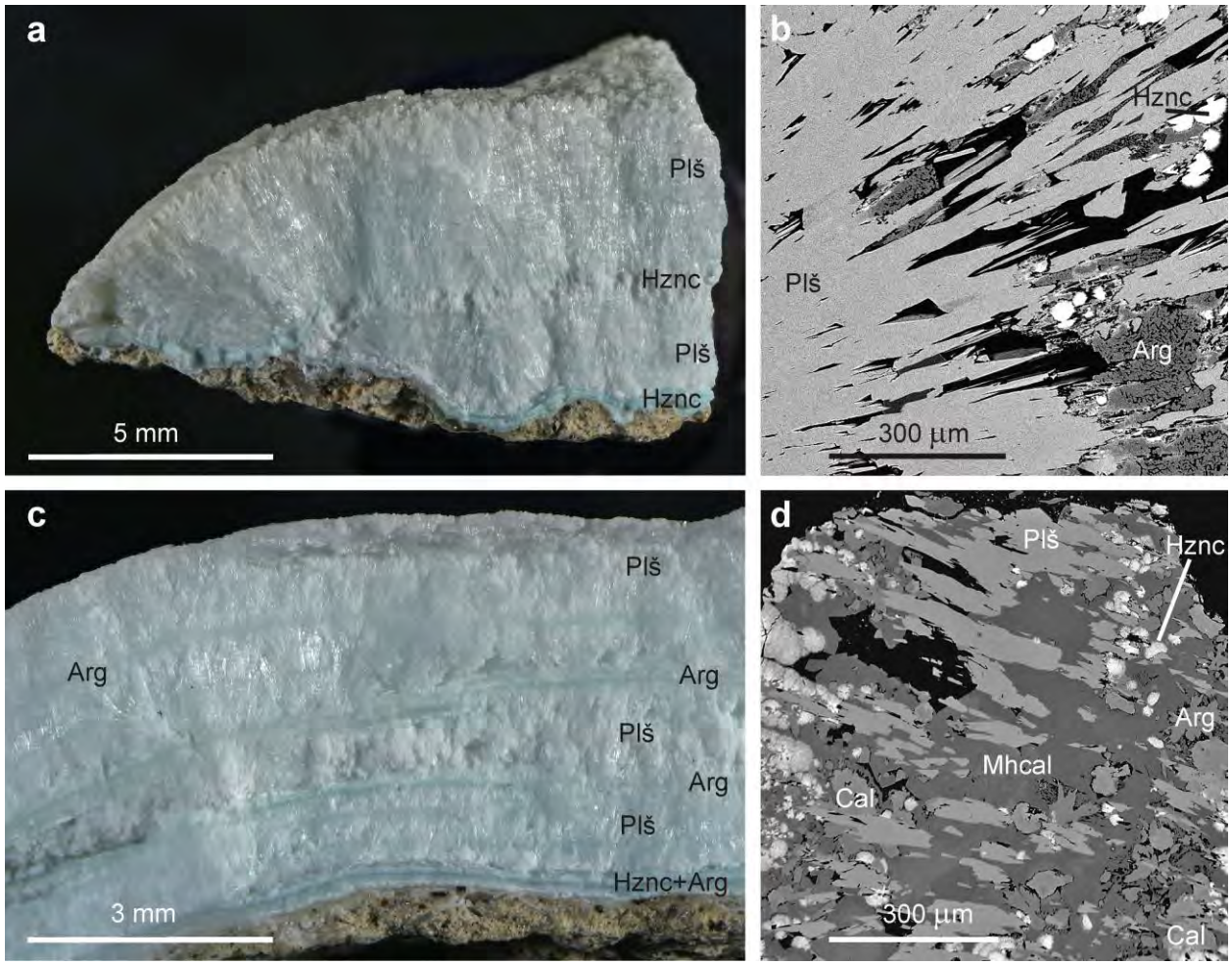

Figure 1. a) Crust formed by acicular paulišite crystals (Plš) with a thin hydrozincite (Hznc) layer and light blue hydrozincite at the contact with rock (holotype sample); **b)** acicular crystals of paulišite with Zn-containing aragonite (Arg) aggregates and hemispherical aggregates of hydrozincite, BSE photo (holotype sample); **c)** paulišite crust with thin layers of fine-grained Zn-bearing aragonite and intergrowths of hydrozincite and aragonite at the contact with rock; **d)** elongated crystals of paulišite in association with calcite (Cal), aragonite and hydrozincite in monohydrocalcite (Mhcal) matrix, BSE photo.

This is the peer-reviewed, final accepted version for American Mineralogist, published by the Mineralogical Society of America.
The published version is subject to change. Cite as Authors (Year) Title. American Mineralogist, in press.
DOI: https://doi.org/10.2138/am-2024-9418. http://www.minsocam.org/

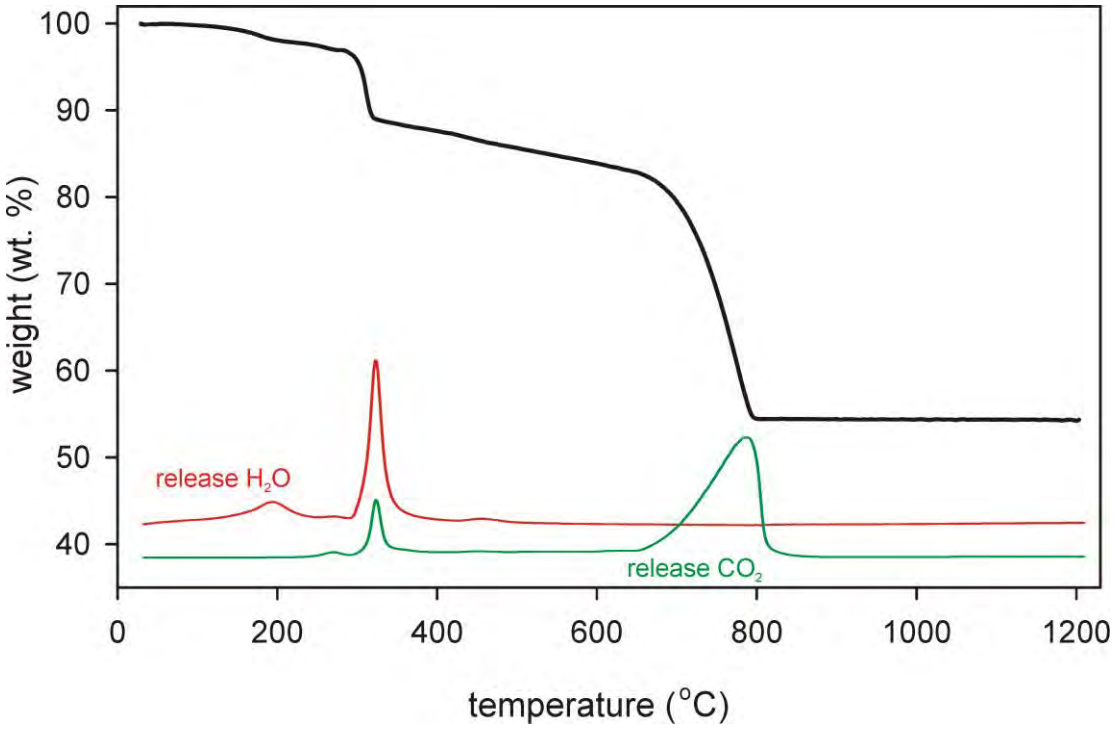

Figure 2. Thermogravimetric curve for paulišite.

This is the peer-reviewed, final accepted version for American Mineralogist, published by the Mineralogical Society of America.
The published version is subject to change. Cite as Authors (Year) Title. American Mineralogist, in press.
DOI: https://doi.org/10.2138/am-2024-9418. http://www.minsocam.org/

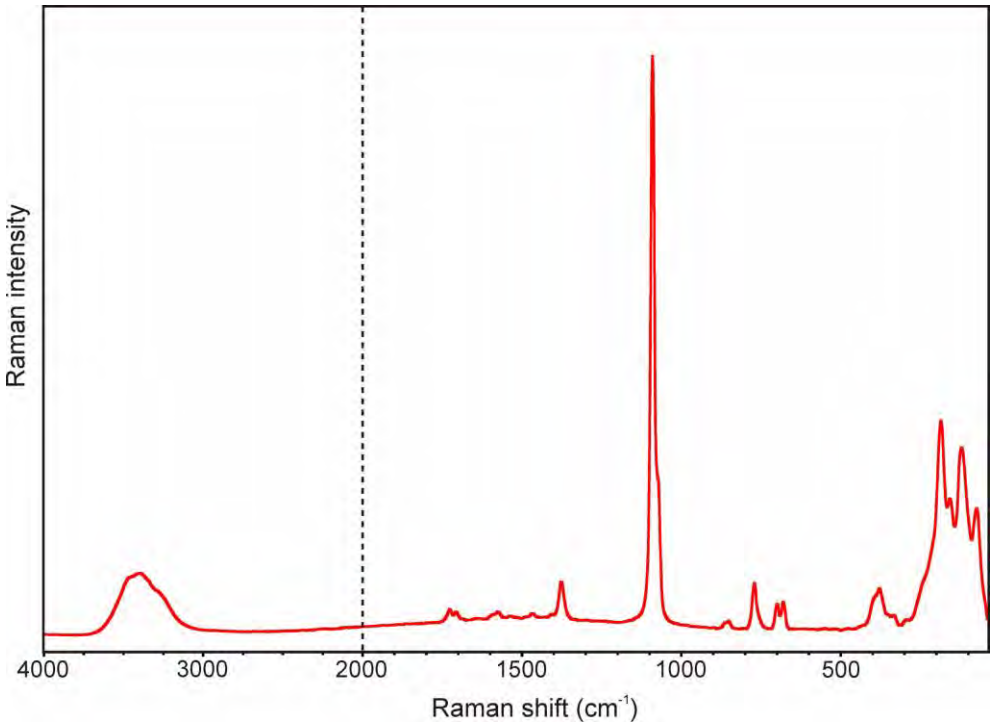

628

629

630 **Figure 3.** Raman spectrum of paulišite in the full range (4000–30 cm^{-1}, split at 2000 cm^{-1}).

631

This is the peer-reviewed, final accepted version for American Mineralogist, published by the Mineralogical Society of America.
The published version is subject to change. Cite as Authors (Year) Title. American Mineralogist, in press.
DOI: https://doi.org/10.2138/am-2024-9418. http://www.minsocam.org/

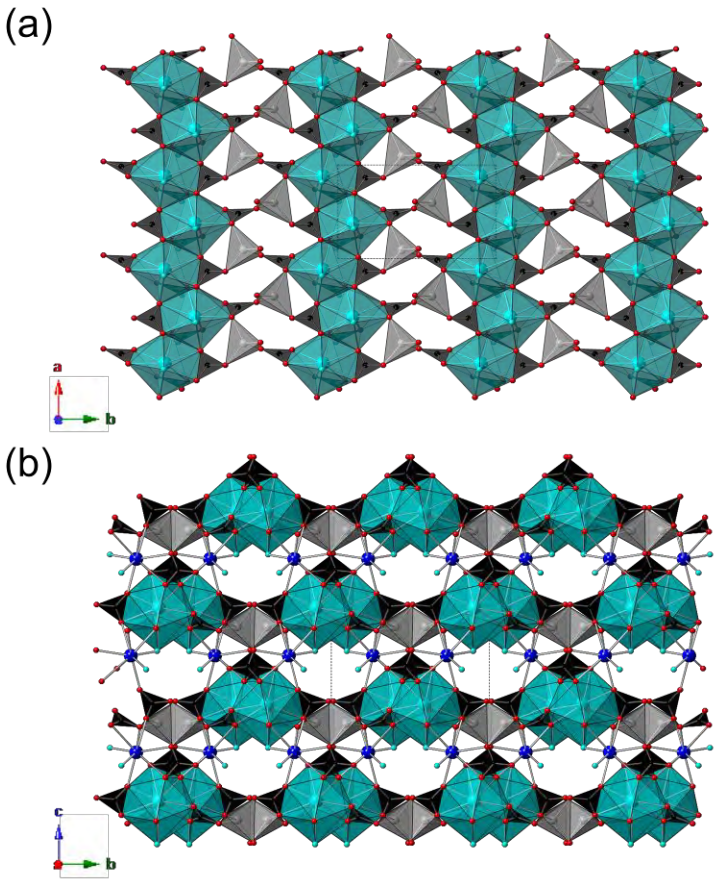

Figure 4. Crystal structure of paulišite. (a) The {001} heteropolyhedral layer as seen down **c**. (b) Structure as seen down **a**, with {001} layers connected through Ca(2) polyhedra, CO_3 groups, and H-bonds (not shown). Zn- and Ca(1)-centered polyhedra are shown in light grey and cyan, respectively, whereas CO_3 groups are shown as black polyhedra. Ca(2) is shown as blue ball-and-sticks. O sites hosting O^{2-} atoms are red circles, whereas sites hosting O atoms belonging to H_2O groups are shown as cyan circles. H atoms are not shown.